

## Global deceleration and inward movements of X-ray knots and rims of RCW 103

HIROMASA SUZUKI,<sup>1</sup> TAKAAKI TANAKA,<sup>1</sup> TSUYOSHI INOUE,<sup>1</sup> HIROYUKI UCHIDA,<sup>2</sup> AND TAKUTO NARITA<sup>2</sup>

<sup>1</sup>*Department of Physics, Faculty of Science and Engineering, Konan University, 8-9-1 Okamoto, Higashinada, Kobe, Hyogo 658-8501, Japan*

<sup>2</sup>*Department of Physics, Kyoto University, Kitashirakawa Oiwake-cho, Sakyo, Kyoto 606-8502, Japan*

Submitted to ApJ

### ABSTRACT

Kinematics of shocks, ejecta knots, and the compact remnant of a supernova remnant gives an insight into the nature of the progenitor and surrounding environment. We report on a proper motion measurement of X-ray knots and rims of the magnetar-hosting supernova remnant RCW 103. Chandra data obtained in three epochs, 1999, 2010, and 2016 are used. We find a global deceleration of 12 knots and rims both in northern and southern regions within the last  $\sim 24$  yrs, even though its age is thought to be larger than 2 kyr. Some of them even changed their moving directions from outward ( $\sim 1,000$  km s<sup>-1</sup>) to inward ( $\sim -2,000$  km s<sup>-1</sup>). Our findings can be explained with a collision with a high-density medium both in the northern and southern edges of the remnant, although the remnant may still be expanding in the wind-blown cavity. The proper motion of the associated magnetar 1E 161348–5055 is possibly detected with a velocity of  $\approx 500$  km s<sup>-1</sup>.

*Keywords:* Supernova remnants (1667); X-ray sources (1822); Shocks (2086); Circumstellar matter (241); Magnetars (992)

### 1. INTRODUCTION

RCW 103 is a young or middle-aged supernova remnant (SNR) hosting the compact object 1E 161348–5055 (Tuohy & Garmire 1980). Its age, i.e., elapsed time after the supernova explosion, is estimated to be 2.0–4.4 kyr (Carter et al. 1997; Braun et al. 2019). It has a nearly circular shape with a spatial extent of  $\sim 10'$  or  $\sim 9$  pc at the estimated distance of 3.1 kpc (Reynoso et al. 2004). Interestingly, its morphologies are similar among radio, infrared, optical, and X-rays. All show bright emissions in the southern large area and northern small part. Radio continuum observations revealed a smooth structure without clear shells (Dickel et al. 1996). Paron et al. (2006) found an interacting <sup>12</sup>CO cloud in the southern area. Infrared observations also found interacting H<sub>2</sub> gas and other elements (Oliva et al. 1990, 1999; Rho et al. 2001; Reach et al. 2006; Pinheiro Gonçalves et al. 2011). A 1720 MHz OH maser

detection from the southern area also supports the cloud interaction (Frail et al. 1996). Carter et al. (1997) detected H $\alpha$  filaments from both south and north, with the northern filament being much fainter. They estimated the age to be  $\sim 2$  kyr based on optical proper motions of  $\sim 1,100$  km s<sup>-1</sup>.

The compact object 1E 161348–5055 has been known as an extraordinary compact object with a very long periodicity  $\sim 6.67$  h (De Luca et al. 2006). In 2016, it exhibited a bursting activity and began to be recognized as a magnetar (D’Aì et al. 2016; Rea et al. 2016; Tendulkar et al. 2017). Previous X-ray observations shed light on the relation between the progenitor and magnetar (Nugent et al. 1984; Frank et al. 2015; Braun et al. 2019; Zhou et al. 2019). A common conclusion is that the supernova explosion was less energetic (with an explosion energy of  $10^{49}$ – $10^{50}$  erg) and the progenitor was not very massive ( $\lesssim 13 M_{\odot}$ ). Most recently, Narita et al. (2023) identified X-ray emission from shock-heated circumstellar medium (CSM) near the edges of RCW 103. They found an enhanced N/O abundance ratio ( $\sim 4$ ) of the CSM, and suggested that the progenitor rotation was not rapid ( $\lesssim 100$  km s<sup>-1</sup>) and a magnetar forma-

tion by dynamo effects in massive stars ( $> 35 M_{\odot}$ ) is unlikely.

From another aspect, constraining the X-ray kinematic properties including movements of forward shocks, ejecta knots, and the associated magnetar is of great importance as well to understand the nature of the progenitor and magnetar. In this paper, we report on proper motion measurements of X-ray bright knots and rims, and the associated magnetar. Our original purpose was to determine the explosion center and obtain tight constraints on the age and kinematics. However, we find a global deceleration and inward movements of the X-ray knots and rims. In Section 2, we summarize the observation log and data reduction processes. Our proper motion analysis and results are described in Section 3. We discuss the origin of the deceleration and inward movements in Section 4, and conclude in Section 5.

## 2. OBSERVATION AND DATA REDUCTION

We use five Chandra ACIS-I (Garmire 1997) observations of the RCW 103 region listed in Table 1, which consist of three epochs (1999, 2010, and 2016). The baselines for the proper motion study are  $\approx 11$  yr and  $\approx 6$  yr, for the first and second intervals, respectively. The observation log is summarized in Table 1.

We use the analysis software CIAO (v4.15; Fruscione et al. 2006) and calibration database v4.10.2 for the data reduction and analysis. We process the raw data using the standard data reduction method (`chandra_repro`).

## 3. ANALYSIS AND RESULTS

We perform a proper motion study on RCW 103. The procedures and results are presented in this section. In our analysis, we use the software HEASoft (v6.30.1; HEASARC 2014), XSPEC (v12.12.1; Arnaud 1996), and AtomDB 3.0.9. Throughout the paper, uncertainties in the text, figures, and tables indicate  $1\sigma$  confidence intervals.

Figure 1 presents an X-ray image of the whole remnant with our analysis regions. We choose bright knots and sharp edges as our analysis regions. The profile extraction directions are determined by eye to roughly correspond to the directions perpendicular to the boundaries or toward the geometric center of the remnant.

### 3.1. Aspect correction

To maximize the reliability and accuracy of the proper motion measurement, we perform the aspect correction to individual observations. As a large fraction of the central region of the field of view is covered by the bright target source, we only find 7–9 point-like sources with

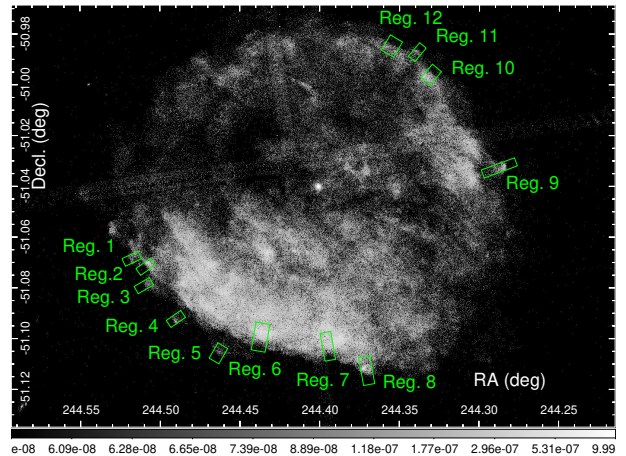


**Figure 1.** Exposure-corrected Chandra image of RCW 103 in the energy band of 0.5–5.0 keV. The radial-profile extraction regions are indicated with the green boxes.

off-axis angles of  $> 4'$ . We perform the correction with the CIAO tool `wcs_match` and `wcs_update`. Considering the small number of detected point-like sources and their off-axis positions, we perform coordinate transformations without rotation and scaling. The resultant transformation parameters are listed in Table 1. The relative offsets of 0.1–0.6 pixels, which correspond to  $0''.05$ – $0''.3$ , are reasonable according to the pointing accuracy of Chandra ACIS-I,  $\approx 0''.67$ .<sup>1</sup>

### 3.2. Proper motions of X-ray knots and rims

We measure proper motions using radial profiles extracted from the regions indicated in Figure 1. The two observations in 2010 are merged after the aspect correction. The same process is done for the observations in 2016. Thus, hereafter, we use three images obtained in 1999, 2010, and 2016. Flux profiles are extracted from the exposure-corrected images in the 0.5–5.0 keV energy range. Two examples are shown in Figure 2 (a-1) and (b-1).

We use the same method as that taken in Tanaka et al. (2021) and Suzuki et al. (2022) in calculating the velocities. Two profiles obtained from two epochs are used. We artificially shift the second profile by  $\Delta x$  and evaluate the difference against the first one with  $\chi^2(\Delta x)$ , which is defined as

$$\chi^2(\Delta x) = \sum_i \frac{(f_i - g_i(\Delta x))^2}{\Delta f_i^2 + \Delta g_i(\Delta x)^2}, \quad (1)$$

where  $f_i$  and  $\Delta f_i$  indicate the flux and error of the bin number  $i$  in the first observation, and  $g_i$  and  $\Delta g_i$  indi-

<sup>1</sup> The reference for the pointing accuracy is <https://cxc.harvard.edu/cal/ASPECT/celmon/>.

**Table 1.** Chandra observation log

ObsID	R.A. (2000)	Dec. (2000)	Date	Exposure (ks)	$\Delta x$ (pixel) <sup>a</sup>	$\Delta y$ (pixel) <sup>a</sup>
123	244°40550	51°02022	1999 Sep. 26	13.4	0.51	0.39
11823	244°41094	51°02284	2010 Jun. 01	62.5	...	...
12224	244°40770	51°02419	2010 Jun. 27	17.8	-0.10	0.13
18459	244°41579	51°04894	2016 May 23	25.8	... <sup>b</sup>	... <sup>b</sup>
18854	244°41333	51°04969	2016 May 30	13.0	-0.64	0.29

<sup>a</sup>Coordinate transformation parameters with respect to those of ObsID 11823. Transformation directions  $+\Delta x$  and  $+\Delta y$  correspond to  $-R.A.$  and  $+Dec.$ , respectively.

<sup>b</sup>No correction is performed due to the low quality of point-like sources.

cate those of the shifted second profile. This calculation is repeated with various values of  $\Delta x$  and we obtain  $\chi^2$  as a function of  $\Delta x$ . The minimum  $\chi^2$  value ( $\chi_{\min}^2$ ) and corresponding shift ( $\Delta x_{\min}$ ) are determined by fitting the  $\chi^2-\Delta x$  plot with a parabola function. We calculate proper motion velocity from the best-fit  $\Delta x_{\min}$  and known baselines. The profile shift is not limited to an integer multiple of the bin width. We re-bin the shifted profile  $g(\Delta x)$  with the same bin arrangement as  $f$  with an assumption of a uniform probability distribution inside each bin. Then, the profile-shift ranges that give  $\chi^2(\Delta x) = \chi_{\min}^2 + 1$  are calculated from the best-fit parabola functions. These ranges are considered to be  $1\sigma$  confidence ranges of the profiles shifts.

The  $\chi^2-\Delta x$  plots of Reg. 5 and Reg. 6 are shown in Figure 2 (a-2) and (b-2), respectively. The  $\Delta x_{\min}$  values in the second interval (2010 to 2016) are negative, whereas those in the first (1999 to 2010) are positive. These indicate that their movements were outward before 2010 but they changed their moving directions to inward after 2010. We show the calculated velocities of all the analysis regions in the two intervals in Table 2 and Figure 3. One can see a global deceleration from the first to second interval. Among them, Regs. 5–8 are firmly found to be moving inward in the second interval.

We here evaluate possible systematic uncertainties. The pointing accuracy of Chandra has to be considered, which would be  $< 0''.67$  after the aspect correction. Even if we assume that the astrometry offsets between the images are significant, some of the knots or rims still should be moving inward in the second interval, because the analysis regions include both northern and southern edges. The profile extraction directions are determined by eye, and thus the measured velocities will have some uncertainties due to deviations from the true moving directions. We evaluate this uncertainty by slightly changing the extraction direction ( $\pm 10$  deg) of Reg. 6, finding a  $\lesssim 100$  km s<sup>-1</sup> variation in velocities. This uncertainty is not significant because the statistical uncertainties are much larger. We also repeat the analysis procedure with

1) an alternative aspect correction with an optical source catalog and 2) different extraction energy ranges of 1.0–5.0 keV and 1.5–5.0 keV. The measured velocities are largely consistent with the ones obtained above with the same tendency (See Appendix A and B).

**Table 2.** Proper motion velocities<sup>a</sup>

Region	Velocity (km s <sup>-1</sup> )	
	1999–2010	2010–2016
Reg.1	1000 ± 600	-1000 ± 1000
Reg.2	1400 ± 300	-600 ± 500
Reg.3	1600 ± 600	-1100 ± 800
Reg.4	990 ± 400	-500 ± 400
Reg.5	1600 ± 600	-2100 ± 700
Reg.6	1100 ± 300	-1300 ± 500
Reg.7	-10 ± 500	-1500 ± 800
Reg.8	1100 ± 300	-1500 ± 500
Reg.9	60 ± 400	-100 ± 500
Reg.10	880 ± 400	-600 ± 600
Reg.11	1400 ± 500	-70 ± 700
Reg.12	1200 ± 400	-1200 ± 800

<sup>a</sup>A distance of 3.1 kpc is assumed. Minus velocities indicate inward movements (Same for Table 3 and 4).

### 3.3. Proper motion of the associated magnetar 1E 161348–5055

Using the aspect-corrected, 0.5–5.0 keV images, we measure the proper motion of the associated magnetar, 1E 161348–5055. For individual observations, we determine the positions of the magnetar and their statistical errors using the CIAO tool `wavdetect`. The determined locations are presented in Figure 4. The angular displacement between 1999 and 2016 (ObsID 18854) is measured to be  $0''.585 \pm 0''.025$ , which is converted to  $501 \pm 21$  km s<sup>-1</sup> at a distance of 3.1 kpc (Reynoso et al. 2004). We note that this displacement might be insignif-

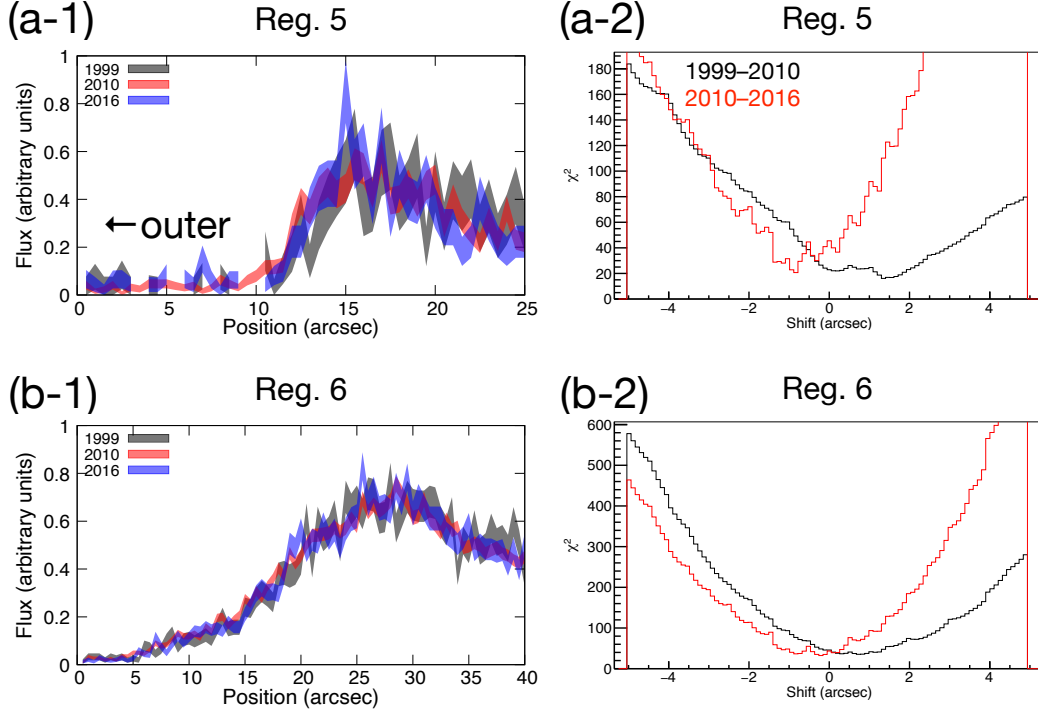


**Figure 2.** Radial profiles and derived  $\chi^2 - \Delta x$  (shift) plots extracted from Reg. 5 (a) and from Reg. 6 (b). In the radial profiles, negative directions correspond to outer regions. In the  $\chi^2 - \Delta x$  plots, positive values indicate outward movements.

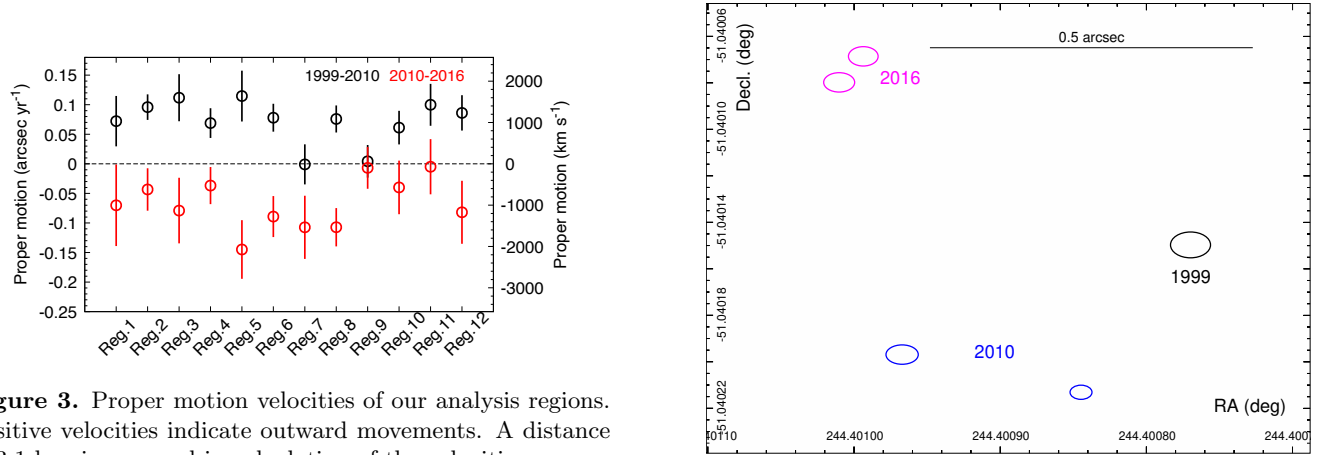


**Figure 3.** Proper motion velocities of our analysis regions. Positive velocities indicate outward movements. A distance of 3.1 kpc is assumed in calculation of the velocities.

icant if we consider systematic uncertainties due to the pointing accuracy.

#### 4. DISCUSSION

We find a global deceleration of the X-ray knots and rims in RCW 103 in the last  $\sim 24$  yrs, even though its age is thought to be larger than 2 kyr. Some of them were even moving inward in the second interval, from 2010 to 2016. We here discuss the origin of this sudden deceleration.

Narita et al. (2023) proposed that X-ray emitting plasma near the outer edges are CSM dominated. They

**Figure 4.** Locations of the magnetar 1E 161348-5055 in 1999, 2010, and 2016. The central positions and radii of the ellipses indicate the estimated positions of the magnetar at different times and their statistical errors.

also suggested that the remnant is still expanding in the wind-blown bubble based on the derived progenitor properties. The X-ray bright southern and northern edges, on which this work focuses, coincide with the locations of H $\alpha$  emission (Carter et al. 1997). The southern edge is thought to be interacting with a molecular cloud (Dickel et al. 1996). Considering these facts and suggestions, we propose a scenario that both northern and southern regions interact with molecular or atomic

clouds, although the remnant is still expanding in the wind-blown bubble. We assume that the northern part is also interacting with a high-density medium but it is yet to be detected. The weaker H $\alpha$  emission and slower deceleration in the northern part support an interpretation that the interacting medium there has a lower density than the southern part.

Regs. 5–8 are found to have decelerated from  $\sim +1,000$  km s $^{-1}$  (outward) to  $\sim -2,000$  km s $^{-1}$  (inward). This can be interpreted as a reflection of the shocks due to a collision with a high-density medium. The shock reflection by an interaction with a high density cloud is studied analytically by Miesch & Zweibel (1994) and Inoue et al. (2012). For a high Mach number incident shock, like an SNR blast wave shock, the relation between the incident/reflection shock velocities and density jump at a cloud surface is given by eq. (A3) of Inoue et al. (2012). In the case of an incident shock velocity  $\sim 1,000$  km s $^{-1}$  and a reflection shock velocity  $\sim -2,000$  km s $^{-1}$ , the required density jump is calculated to be  $\sim 36$ . This is consistent with a typical density jump between a diffuse ISM and HI clouds. We note that a shock wave can be reflected whereas shock-heated plasma will not be. The reflected shock enhances thermal X-rays while moving inward, which can be observed as an inward movement if the newly enhanced emission is bright enough. If the observed X-ray radial profiles originate from mixtures of outward- and inward-moving plasma, actual reflected-shock velocities in the observer’s frame might be larger than the measured velocities.

Inward moving filaments were found in a few other young SNRs, such as Cassiopeia A (Sato et al. 2018) and RCW 86 (Suzuki et al. 2022). The inward filaments are interpreted as reverse shocks for Cassiopeia A and reflection shocks for RCW 86. The case of RCW 103 is similar to RCW 86. A large difference is the locations where the inward movements are observed: in the present case, they are at the outer edges of the X-ray emission, whereas they are well behind outermost filaments in the case of RCW 86. This is consistent with our interpretation, a very recent collision in RCW 103.

To summarize, the global deceleration can be understood as a result of a collision of the shocks with a high-density medium (molecular or atomic cloud), although the X-ray emitting plasma may still be expanding in the wind-blown bubble.

## 5. CONCLUSION

We examined proper motions of X-ray knots and rims in the southern and northern edges of RCW 103. We found a global deceleration of them within the last  $\sim 24$  yrs, even though its age is thought to be larger than 2 kyr. Among them, Regs. 5–8 were found to have changed the moving directions from  $\sim +1,000$  km s $^{-1}$  (outward) to  $\sim -2,000$  km s $^{-1}$  (inward). We confirmed that the deceleration and inward movements are robust to the uncertainties in the moving directions and the pointing accuracy of Chandra. The inward movements can be understood as a shock reflection due to a collision with a high-density medium. As a conclusion, the global deceleration can be explained as due to a collision with a high-density medium both in the northern and southern regions, although the X-ray emitting plasma may still be expanding in the wind-blown bubble.

- 1 We appreciate a fruitful discussion with H. Sano about
- 2 the surrounding medium. This research has made
- 3 use of the VizieR catalogue access tool, CDS, Stras-
- 4 bourg, France (DOI : 10.26093/cds/vizieR). The origi-
- 5 nal description of the VizieR service was published
- 6 in 2000, A&AS 143, 23. This work was partially
- 7 supported by JSPS/MEXT grant Nos. JP21J00031
- 8 (HS), JP19H01936, JP21H04493 (TT), and JP22H01265
- 9 (HU).

*Facilities:* Chandra

*Software:* HEASoft (v6.30.1; HEASARC 2014), CIAO (v4.15; Fruscione et al. 2006)

## APPENDIX

### A. ASPECT CORRECTION WITH THE NOMAD-1 OPTICAL SOURCE CATALOG

In order to evaluate systematic uncertainties associated with the aspect correction, we here apply another aspect correction. We use the NOMAD-1 optical source catalog (Zacharias et al. 2004) available via the VizieR service<sup>2</sup> (Ochsenbein et al. 2000) to register the point-like sources in the Chandra images. We find 4–6 X-ray sources (depending

<sup>2</sup> <https://doi.org/10.26093/cds/vizieR>

on observations) which match the catalog sources. After correcting all the images, we measure the proper motions in the same way as in Section 3. The resultant velocities are listed in Table 3. Overall, the velocities are consistent with the ones obtained in Section 3, suggesting that the systematic uncertainties due to the aspect correction are small compared to the statistical errors.

**Table 3.** Proper motion velocities in the alternative aspect correction case

Region	Velocity (km s <sup>-1</sup> )	
	1999–2010	2010–2016
Reg.1	1300 ± 500	−3000 ± 1000
Reg.2	1100 ± 300	−1500 ± 500
Reg.3	1100 ± 600	−2100 ± 800
Reg.4	900 ± 400	−1600 ± 500
Reg.5	1700 ± 600	−2400 ± 700
Reg.6	1300 ± 300	−900 ± 500
Reg.7	400 ± 500	−1300 ± 700
Reg.8	1400 ± 300	−400 ± 500
Reg.9	600 ± 400	1400 ± 600
Reg.10	900 ± 400	−100 ± 700
Reg.11	800 ± 500	400 ± 700
Reg.12	1500 ± 400	−900 ± 800
Reg.13	100 ± 800	−2900 ± 1200

## B. PROPER MOTIONS IN DIFFERENT ENERGY RANGES

We here check for systematic uncertainties of the proper motions due to the extraction energy range. Because the detector calibration might be less reliable at low energies due to the contamination on the sensor surface (Marshall et al. 2004; O’Dell et al. 2015; Plucinsky et al. 2018), we test two additional cases where we use the 1.0–5.0 keV and 1.5–5.0 keV energy ranges. The measured velocities are listed in Table 4. In the latter case, velocities are constrained only for Regs. 6, 7, and 8, due to the limited statistics. In both cases, one can see that the results are mostly consistent with the ones in Section 3, showing a global deceleration and a change in moving directions.

## REFERENCES

- Arnaud, K. A. 1996, in *Astronomical Society of the Pacific Conference Series*, Vol. 101, *Astronomical Data Analysis Software and Systems V*, ed. G. H. Jacoby & J. Barnes, 17
- Braun, C., Safi-Harb, S., & Fryer, C. L. 2019, *MNRAS*, 489, 4444, doi: [10.1093/mnras/stz2437](https://doi.org/10.1093/mnras/stz2437)
- Carter, L. M., Dickel, J. R., & Bomans, D. J. 1997, *PASP*, 109, 990, doi: [10.1086/133971](https://doi.org/10.1086/133971)
- D’Ài, A., Evans, P. A., Burrows, D. N., et al. 2016, *MNRAS*, 463, 2394, doi: [10.1093/mnras/stw2023](https://doi.org/10.1093/mnras/stw2023)
- De Luca, A., Caraveo, P. A., Mereghetti, S., Tiengo, A., & Bignami, G. F. 2006, *Science*, 313, 814, doi: [10.1126/science.1129185](https://doi.org/10.1126/science.1129185)
- Dickel, J. R., Green, A., Ye, T., & Milne, D. K. 1996, *AJ*, 111, 340, doi: [10.1086/117786](https://doi.org/10.1086/117786)
- Frail, D. A., Giacani, E. B., Goss, W. M., & Dubner, G. 1996, *The Astrophysical Journal*, 464, L165, doi: [10.1086/310103](https://doi.org/10.1086/310103)
- Frank, K. A., Burrows, D. N., & Park, S. 2015, *ApJ*, 810, 113, doi: [10.1088/0004-637X/810/2/113](https://doi.org/10.1088/0004-637X/810/2/113)
- Fruscione, A., McDowell, J. C., Allen, G. E., et al. 2006, in *Observatory Operations: Strategies, Processes, and Systems*, ed. D. R. Silva & R. E. Doxsey, Vol. 6270, *International Society for Optics and Photonics (SPIE)*, 586 – 597, doi: [10.1117/12.671760](https://doi.org/10.1117/12.671760)
- Garmire, G. P. 1997, in *American Astronomical Society Meeting Abstracts*, Vol. 190, *American Astronomical Society Meeting Abstracts #190*, 34.04
- HEASARC. 2014, *HEASoft: Unified Release of FTOOLS and XANADU*. <http://ascl.net/1408.004>
- Inoue, T., Yamazaki, R., Inutsuka, S.-i., & Fukui, Y. 2012, *ApJ*, 744, 71, doi: [10.1088/0004-637X/744/1/71](https://doi.org/10.1088/0004-637X/744/1/71)

**Table 4.** Proper motion velocities in the different energy-selection cases

Region	Velocity (km s <sup>-1</sup> )	
	1999–2010	2010–2016
1.0–5.0 keV case		
Reg.1	600 ± 1100	−2000 ± 1100
Reg.2	2200 ± 500	−1000 ± 600
Reg.3	800 ± 900	−300 ± 1000
Reg.4	−500 ± 900	−600 ± 600
Reg.5	1400 ± 900	−1400 ± 900
Reg.6	1700 ± 400	−1309 ± 600
Reg.7	100 ± 600	−1600 ± 900
Reg.8	1200 ± 400	−1600 ± 500
Reg.9	400 ± 500	−400 ± 600
Reg.10	800 ± 500	−500 ± 800
Reg.11	1700 ± 600	100 ± 800
Reg.12	1000 ± 600	−500 ± 900
Reg.13	1400 ± 1100	−3200 ± 1700
1.5–5.0 keV case		
Reg.6	2100 ± 900	−3000 ± 1100
Reg.7	1700 ± 2000	−2300 ± 1500
Reg.8	900 ± 1000	−1100 ± 900

Marshall, H. L., Tennant, A., Grant, C. E., et al. 2004, in Society of Photo-Optical Instrumentation Engineers (SPIE) Conference Series, Vol. 5165, X-Ray and Gamma-Ray Instrumentation for Astronomy XIII, ed. K. A. Flanagan & O. H. W. Siegmund, 497–508, doi: [10.1117/12.508310](https://doi.org/10.1117/12.508310)

Miesch, M. S., & Zweibel, E. G. 1994, *ApJ*, 432, 622, doi: [10.1086/174601](https://doi.org/10.1086/174601)

Narita, T., Uchida, H., Yoshida, T., Tanaka, T., & Tsuru, T. G. 2023, *ApJ*, 950, 137, doi: [10.3847/1538-4357/acccf6](https://doi.org/10.3847/1538-4357/acccf6)

Nugent, J. J., Pravdo, S. H., Garmire, G. P., et al. 1984, *ApJ*, 284, 612, doi: [10.1086/162444](https://doi.org/10.1086/162444)

Ochsenbein, F., Bauer, P., & Marcout, J. 2000, *A&AS*, 143, 23, doi: [10.1051/aas:2000169](https://doi.org/10.1051/aas:2000169)

O’Dell, S. L., Swartz, D. A., Tice, N. W., et al. 2015, in Society of Photo-Optical Instrumentation Engineers (SPIE) Conference Series, Vol. 9601, UV, X-Ray, and Gamma-Ray Space Instrumentation for Astronomy XIX, ed. O. H. Siegmund, 960107, doi: [10.1117/12.2188396](https://doi.org/10.1117/12.2188396)

Oliva, E., Moorwood, A. F. M., & Danziger, I. J. 1990, *A&A*, 240, 453

Oliva, E., Moorwood, A. F. M., Drapatz, S., Lutz, D., & Sturm, E. 1999, *A&A*, 343, 943, doi: [10.48550/arXiv.astro-ph/9901254](https://doi.org/10.48550/arXiv.astro-ph/9901254)

Paron, S. A., Reynoso, E. M., Purcell, C., Dubner, G. M., & Green, A. 2006, *PASA*, 23, 69, doi: [10.1071/AS06003](https://doi.org/10.1071/AS06003)

Pinheiro Gonçalves, D., Noriega-Crespo, A., Paladini, R., Martin, P. G., & Carey, S. J. 2011, *AJ*, 142, 47, doi: [10.1088/0004-6256/142/2/47](https://doi.org/10.1088/0004-6256/142/2/47)

Plucinsky, P. P., Bogdan, A., Marshall, H. L., & Tice, N. W. 2018, in Society of Photo-Optical Instrumentation Engineers (SPIE) Conference Series, Vol. 10699, Space Telescopes and Instrumentation 2018: Ultraviolet to Gamma Ray, ed. J.-W. A. den Herder, S. Nikzad, & K. Nakazawa, 106996B, doi: [10.1117/12.2312748](https://doi.org/10.1117/12.2312748)

Rea, N., Borghese, A., Esposito, P., et al. 2016, *ApJL*, 828, L13, doi: [10.3847/2041-8205/828/1/L13](https://doi.org/10.3847/2041-8205/828/1/L13)

Reach, W. T., Rho, J., Tappe, A., et al. 2006, *AJ*, 131, 1479, doi: [10.1086/499306](https://doi.org/10.1086/499306)

Reynoso, E. M., Green, A. J., Johnston, S., et al. 2004, *PASA*, 21, 82, doi: [10.1071/AS03053](https://doi.org/10.1071/AS03053)

Rho, J., Reach, W. T., Koo, B. C., & Cambresy, L. 2001, in American Institute of Physics Conference Series, Vol. 565, Young Supernova Remnants, ed. S. S. Holt & U. Hwang, 197–200, doi: [10.1063/1.1377094](https://doi.org/10.1063/1.1377094)

Sato, T., Katsuda, S., Morii, M., et al. 2018, *ApJ*, 853, 46, doi: [10.3847/1538-4357/aaa021](https://doi.org/10.3847/1538-4357/aaa021)

Suzuki, H., Katsuda, S., Tanaka, T., et al. 2022, *ApJ*, 938, 59, doi: [10.3847/1538-4357/ac8df7](https://doi.org/10.3847/1538-4357/ac8df7)

Tanaka, T., Okuno, T., Uchida, H., et al. 2021, *ApJL*, 906, L3, doi: [10.3847/2041-8213/abd6cf](https://doi.org/10.3847/2041-8213/abd6cf)

Tendulkar, S. P., Kaspi, V. M., Archibald, R. F., & Scholz, P. 2017, *ApJ*, 841, 11, doi: [10.3847/1538-4357/aa6d0c](https://doi.org/10.3847/1538-4357/aa6d0c)

Tuohy, I., & Garmire, G. 1980, *ApJL*, 239, L107,  
doi: [10.1086/183303](https://doi.org/10.1086/183303)

Zacharias, N., Monet, D. G., Levine, S. E., et al. 2004, in  
American Astronomical Society Meeting Abstracts, Vol.  
205, American Astronomical Society Meeting Abstracts,  
48.15

Zhou, P., Vink, J., Safi-Harb, S., & Miceli, M. 2019, *A&A*,  
629, A51, doi: [10.1051/0004-6361/201936002](https://doi.org/10.1051/0004-6361/201936002)